



Prediction of depinning transitions in interface models using Gini and Kolkata indicesDiksha , Gunnemeda Eswar, and Soumyajyoti Biswas *Department of Physics, SRM University - AP, Andhra Pradesh 522240, India*

(Received 10 October 2023; accepted 12 March 2024; published 5 April 2024)

The intermittent dynamics of driven interfaces through disordered media and its subsequent depinning for large enough driving force is a common feature for a myriad of diverse systems, starting from mode-I fracture, vortex lines in superconductors, and magnetic domain walls to invading fluid in a porous medium, to name a few. In this work, we outline a framework that can give a precursory signal of the imminent depinning transition by monitoring the variations in sizes or the inequality of the intermittent responses of a system that are seen prior to the depinning point. In particular, we use measures traditionally used to quantify economic inequality, i.e., the Gini index and the Kolkata index, for the case of the unequal responses of precritical systems. The crossing point of these two indices serves as a precursor to imminent depinning. Given a scale-free size distribution of the responses, we calculate the expressions for these indices, evaluate their crossing points, and give a recipe for forecasting depinning transitions. We apply this method to the Edwards-Wilkinson, Kardar-Parisi-Zhang, and fiber bundle model interface with variable interaction strengths and quenched disorder. The results are applicable for any interface dynamics undergoing a depinning transition. The results also explain previously observed near-universal values of Gini and Kolkata indices in self-organized critical systems.

DOI: [10.1103/PhysRevE.109.044113](https://doi.org/10.1103/PhysRevE.109.044113)**I. INTRODUCTION**

An interface driven through a disordered medium is a situation that appears in a wide variety of physical systems, such as domain wall dynamics through a disordered magnet [1,2], fluid front invading a disordered porous medium [3,4], vortex lines in superconductors [5,6], and fracture front in mode-I fracture [7,8], to name a few. As the interface is acted upon by an external driving force, the interface will be depinned and will keep moving indefinitely, for a critical value of the force.

The critical value of the driving force needed for the depinning transition is nontrivial, given that the dynamics of the interface is a cooperative phenomenon, mediated by the “elastic” interacting between the parts of the interface. As an interface goes from pinned to moving phases, it is often characterized as a second-order transition (see, however, Ref. [9] that deals with systems that do not fall under this characterization). The tools of critical phenomena, namely, the universality hypothesis, are therefore applicable for such systems and can help in estimating the critical exponent values [10]. However, given the nature of the systems where depinning can occur, it is often also vital to have an estimate for the distance from the imminent transition point, when such a point is approached from the subcritical regime. For example, if the mode-I fracture [7] is studied for a disordered sample, then a depinning transition would imply a catastrophic failure of the sample. Similarly, if the dynamics of a magnetic domain wall [1] is studied using an external magnetic field, a depinning transition would mean a “catastrophic” switching of the magnetic state of the sample (say, from majority up spin to majority down spin) [11]. In the case of fluid flow through porous media [3], depinning would result in a breakthrough of the invading fluid through the medium in question, and so on.

Therefore, much effort has been spent in finding ways to forecast imminent depinning and other similar transitions from the statistical regularities in the response of a system approaching such a transition [12–20]. As mentioned above, depinning transitions are often characterized as (nonequilibrium) critical phenomena, which results in having the possibility of a growing correlation length within the system that in turn, causes cooperative response statistics. Keeping track of this growing correlation, therefore, is a rather non-invasive and optimal monitoring pathway. Specifically, it is known that the dynamics of a system near the depinning transition start showing intermittent behavior. For example, in fracture front propagation, this would be intermittent acoustic energy emissions that have scale-free size distributions [21]. For fluid invasion, the changes in the invaded volume with time would show similar intermittent scale-free statistics (see, e.g., [22]). A similar observation exists for changes in magnetization for magnetic domain wall depinning [23]. It is natural to expect that these intermittent dynamics, together with the scale-free statistics of their “sizes,” would mirror the “health” of the system in terms of their stability or the proximity to a catastrophic (depinning) event.

For the reasons mentioned above, correlation length and time have been used to estimate the vicinity of critical point in many systems. For example, in sandpile models, the temporal and spatial propagation of a small perturbation gives the estimates for correlation time and length, which was used to estimate the distance from the self-organized critical (SOC) state [24]. In Ref. [25], correlation time estimates were made to locate imminent large earthquake events. Other similar analyses for Ising and related models were made as well (see, e.g., [26–28]). However, in all such cases, the correlation length or time is a two-parameter fit, involving the critical point and the critical exponent. In models, one can

make an accurate fit (and hence a precise estimate for the critical point) by doing averages over many ensembles (see, e.g., [24,26,27]). However, in real data, where such averaging does not exist, the limitations in precision are clear (see, e.g., [25,28]). Therefore, it is useful to construct a framework for precursory signals that builds on the noninvasive nature of the measurements of correlation length or time (i.e., estimate the relevant quantities from things such as acoustic emissions), but produces a signal that is not reliant on averaging over ensembles.

In recent years, some attempts were made to anticipate the imminent critical point in a system by quantifying how unequal the responses of a system are as the system approaches the critical point [29,30]. In all cases, the quantification of inequality (or variation) in the “sizes” of response (for example, the unequal avalanche sizes for fracture) is a central requirement. In order to do this quantification, we borrow the idea of inequality indices that are traditionally used in socioeconomic systems, namely, the Lorenz curve [31] and the inequality indices derived from it. For our purposes here, we will use two such quantities: the Gini index (g) [32] and the Kolkata index (k) [33]. The inequality of responses (say, susceptibility in Ising model) would grow as the critical point is approached. Consequently, the inequality indices (g and k measured for the response function) would also grow. The scaling behavior of these inequality indices was shown to exhibit universal properties [30,34–36], and it is also known that g and k of such response functions would cross slightly away from the critical point.

It is, however, not well understood whether the above calculations would be applicable for a time series of a response function (say, avalanches) that is not strictly monotonic as the critical point is approached. In other words, the aim of the present work is to investigate the broader applicability of the methods mentioned above for driven disordered systems, which are vital by virtue of the catastrophic transitions associated with them. We study the Edwards-Wilkinson (EW) [37], Kardar-Parisi-Zhang (KPZ) [38], and fiber bundle interface model (FBM) [39,40] in their precritical states and show that the precursory signals appear, for every single realization of the models, just prior to the depinning transition point. This makes the framework broadly applicable (for nonequilibrium systems with nonmonotonic responses) and reliable.

II. QUANTIFICATION OF INEQUALITY OF AVALANCHES: THE INEQUALITY INDICES

Inequality in the distribution of resources, such as income or wealth, is a common issue in societies. Therefore, the quantification of inequality was a natural question in social sciences. Over the years, several indices were proposed to quantify inequality. For instance, the Gini index (g) [32] (which assesses wealth inequality) and the more recently introduced Kolkata index (k) [33], among others, are used for such quantification. Both of these inequalities are quantified through the Lorenz curve $\mathcal{L}(p)$ [31]. The Lorenz curve denotes that the p smallest fraction of the events accounts for the $\mathcal{L}(p)$ fraction of the total events. In terms of wealth, the poorest p fraction of the individuals own $\mathcal{L}(p)$ fraction of the total wealth. Along the same line, the definition could be

extended to other (non-negative) quantities, such as an avalanche time series, where the Lorenz curve would denote p fraction of the smallest avalanches accounting for $\mathcal{L}(p)$ fraction of the total avalanche mass.

The two inequality indices g and k are then defined through the Lorenz function [31]: with $g = 1 - 2 \int_0^1 \mathcal{L}(p) dp$ and solving the fixed point $1 - k = \mathcal{L}(k)$, respectively (see the Appendix for a detailed discussion).

The Lorenz curve $\mathcal{L}(p)$ is typically represented as a non-linear curve that always lies below the line of perfect equality [diagonal from (0,0) to (1,1)], which represents a situation where all avalanches (or events) have equal size. The Gini index is the area between the equality line and the Lorenz curve, normalized by the area under the equality line (1/2). The range of g varies between 0 to 1, where $g = 0$ corresponds to perfect equality (all sizes are equal) and $g = 1$ corresponds to extreme inequality (all but one size is nonzero). The Kolkata index says that the $1 - k$ fraction of the largest avalanche accounts for the k fraction of total damages (avalanche mass), and the range of k varies between 0.5 to 1, where $k = 0.5$ implies complete equality and $k = 1$ indicates the extreme inequality. This is a generalization of the Pareto’s 80-20 law [41].

These inequality measures have recently been used in physical systems for various different purposes [29,34,42]. As mentioned before, the critical scaling properties [35], prediction of catastrophic events [29], etc. could be studied using these measures. In this work, we calculate these inequality measures of time series of avalanche sizes for multiple models of interface depinning in the subcritical regime. Using the inequalities or variations of sizes between the avalanches in the subcritical phase of the models, we attempt to infer a precursory signal that can work for driven interfaces with a broad class of interaction kernels and for each individual sample, independent of ensemble average.

As indicated above, both of the indices (g and k) that we are interested in need to be evaluated from the Lorenz function $\mathcal{L}(p)$. Now, from a time series with $m + 1$ number of terms, of a variable that follows a power-law size distribution function [assume $P(S) = CS^{-\delta}$; more realistically, lower and upper cutoffs are necessary], the Lorenz function can be estimated in the following way. First we arrange the series in ascending order of the size of the avalanche. Note that this is an approximation, since the actual time series [see Fig. 1(a)] is not strictly monotonically increasing, but the avalanche size increases on average. Nevertheless, the ordering implies

$$S_0 \leq S_1 \leq S_2 \cdots \leq S_m. \quad (1)$$

Then, the number of events with size higher than or equal to S_r is [43]

$$\int_{S_r}^{\infty} P(S) ds = m - r. \quad (2)$$

Assuming $P(S) = CS^{-\delta}$, then

$$S_r^{(1-\delta)} \propto m - r, \quad (3)$$

implying

$$S_r \propto (m - r)^{1/(1-\delta)}. \quad (4)$$

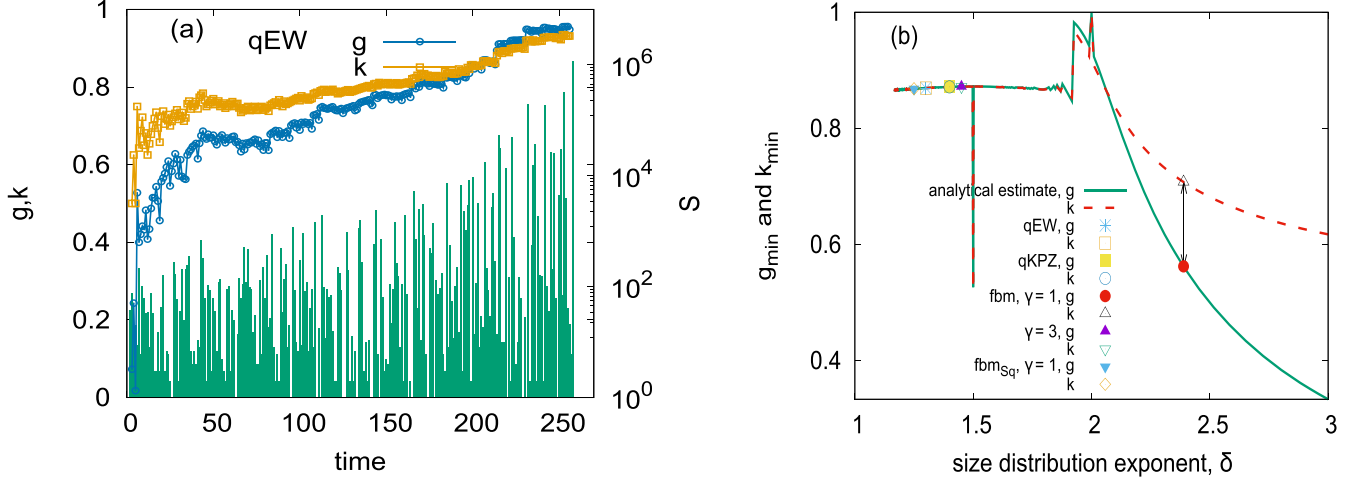


FIG. 1. (a) The time series of avalanche sizes (in logarithmic scale) is shown along with the time variations of g and k for the quenched Edwards-Wilkinson model as a prototype. Here the crossing of g and k can serve as a good indicator of an imminent depinning transition. (b) g_{\min} and k_{\min} are the values where g and k come closest to each other at the earliest time. As can be seen, for $\delta > 2$, they do not cross. For $\delta < 2$, except at $\delta = 1.5$, $g_{\min} = k_{\min} < 1$, which means g and k are expected to cross each other prior to depinning. The points indicate the values at which different models are expected to exhibit this precursory warning. It is seen that different models (EW, KPZ, FBM, and the square of avalanches in FBM) show g_{\min} and k_{\min} values that are nearly universal at about 0.87, which are numerically verified later. The reason for considering the square of avalanches for the FBM interface is discussed later.

For $\delta > 1$, we can write

$$S_r \propto (m - r)^{-n}, \quad (5)$$

with $n = \frac{1}{\delta-1}$, where S_r is the ordered series of avalanche size and r is the rank of avalanche size. Of course, the maximum size (S_m), occurring at $r = m$, is not infinite in physical systems, but limited by an upper cutoff, typically an exponential round-off governed by the system size.

Now, we are interested in dynamical monitoring of the values of g and k , which requires that we only look up to a fraction (say, b) of the whole time series and evaluate \mathcal{L} (and g, k), as b goes from 0 (start time) to 1 (depinning time). Note that we always begin monitoring from the starting time of loading ($b = 0$). Therefore, $g(b)$ and $k(b)$ estimate the inequality of all avalanches that took place from the starting point up to the b fraction of the depinning time. This makes these quantities cumulative measures of inequality. At this point, a crucial observation for further progress in the calculation is that since we are looking at the precritical dynamics of the depinning transition, the time series of avalanches is not stationary. Furthermore, given that we are progressively loading the system without dissipation, the avalanche sizes, on average, will continue to grow, as the depinning point is approached. This is captured in Fig. 1(a). Therefore, for practical purposes, it is a fair assumption to make that until any point of time, the actual avalanche series and that obtained after arranging such series in the ascending order of the avalanche sizes are close to each other at least in terms of measuring g and k (see Fig. 7 for a comparison). We, therefore, proceed to make the estimate of the Lorenz function (and consequently that of g and k) from the ordered functional form of Eq. (5), keeping in mind, however, that nonmonotonicity in avalanche

sizes might affect the g and k crossing point, and that such nonmonotonicity might be different for different models.

Then, the Lorenz function for a time series up to b fraction (where $b = 1$ implies the transition point) can be obtained from (see, also, [35])

$$\mathcal{L}(p, b, n) = \frac{\int_0^{pbm} (m - r)^{-n} dr}{\int_0^{bm} (m - r)^{-n} dr}, \quad (6)$$

putting $m - r = x$ and, upon changing the limits, Eq. (6) becomes

$$\mathcal{L}(p, b, n) = \frac{\int_m^{m-pbm} x^{-n} dx}{\int_m^{m-bm} x^{-n} dx}, \quad (7)$$

which gives

$$\mathcal{L}(p, b, n) = \frac{(m - pbm)^{-n+1} - m^{-n+1}}{(m - bm)^{-n+1} - m^{-n+1}}, \quad (8)$$

which takes the form

$$\mathcal{L}(p, b, n) = \frac{1 - (1 - pb)^{1-n}}{1 - (1 - b)^{1-n}}. \quad (9)$$

It is then straightforward to evaluate the Gini index as

$$g(b, n) = 1 - 2 \int_0^1 \mathcal{L}(p, b, n) dp, \quad (10)$$

after substituting the value of $\mathcal{L}(p, b, n)$ from Eq. (9),

$$g(b, n) = 1 - \frac{2}{1 - (1 - b)^{1-n}} \int_0^1 1 - (1 - pb)^{1-n} dp, \quad (11)$$

which gives, on simplification,

$$g(b, n) = 1 - \frac{2}{1 - (1 - b)^{1-n}} \left[1 + \frac{(1 - b)^{2-n} - 1}{(2 - n)b} \right]. \quad (12)$$

The Kolkata index needs to be obtained from the self-consistent solution of

$$1 - k(n, b) = \mathcal{L}[k(n, b)], \quad (13)$$

which gives

$$1 - k(n, b) = \frac{1 - [1 - k(n, b)b]^{1-n}}{1 - (1 - b)^{1-n}}. \quad (14)$$

Remembering that $n = 1/(\delta - 1)$, with δ the size distribution exponent for the avalanches, we can now evaluate g and k as functions of b , which is a proxy of time. Therefore, we end up with an estimate of time variation of the inequality indices prior to the depinning transition point. It is then necessary to estimate a precursory signal from the time variation of these two indices. As mentioned before, for sufficiently small values of δ , these two indices would cross each other before depinning (i.e., for $b < 1$). In Fig. 1(b), we show the values of the two indices (denoted by g_{\min} and k_{\min}) when they become closest to each other for the lowest value of b , i.e., at the earliest time. This means that if the closest approach of g and k happens for $b < b_0$ and again at $b = b_1$ with $b_0 < b_1$, we then keep the values (g_{\min} and k_{\min}) for b_0 . Now, it is seen that for $\delta > 2$, g and k do not become equal ($g_{\min} \neq k_{\min}$), i.e., there is a finite gap even at $b = 1$. For other values of δ , except at some special cases, the two indices become equal for $b < 1$. The equality of g and k prior to the transition point is then a precursory signal of an imminent depinning transition point.

We have indicated a few points in the plots of Fig. 1(b) that correspond to the expected values of g_{\min} and k_{\min} for different models. For the cases where the avalanche size distribution exponent is steeper than -2 , there will be no crossing of g and k . But one can then consider the square of the avalanche sizes, which will have a shallower size distribution and will therefore have a crossing point. We will discuss the relevant cases of the individual models in the subsequent sections.

One final point to note before moving to the individual models is the near-constant values of g_{\min} and k_{\min} for different values of $\delta < 2$ (excluding $\delta = 1.5$). This range of δ values is observed in a very wide range of physical and socioeconomic systems, especially in the context where they are stipulated to be in a self-organized critical (SOC) state. A measure of g and k for such systems, using a reasonable long-time series that will be in a stationary state, will yield values close to 0.87, as can be seen in Fig. 1(b). This is precisely what was observed in the data quite extensively [30,33] (see, also, [44,45] for citation of scientists) and also in simulations (see, e.g., [36]).

III. MODELS AND METHODS

We now apply the methods outlined so far for three models of depinning transition: the fiber bundle interface model [39,40], the quenched Edwards-Wilkinson model [37], and the quenched Kardar-Parisi-Zhang model [38]. While the frameworks presented here are general, we choose these models since they are paradigmatic models of interface depinning.

A. Simulation methods

Here we outline the details of the simulation methods for different kinds of interfaces that we consider, particularly the fiber bundle interface, and quenched Edwards-Wilkinson and KPZ interfaces. Through intermittent dynamics prior to depinning, the avalanche statistics are recorded and subsequently used to measure the inequality or the variation in their sizes.

1. Simulating FBM

For the fiber bundle model version of the interface [39], we consider an array of discrete elements, each having a finite failure threshold (σ_{th}), drawn from some distribution function. When a load is applied on the interface, some of these elements (fibers) break and the load carried by those fibers is redistributed among the intact fibers. Those fibers can then break, given that the load level has now increased, triggering an avalanche. The avalanche will subsequently stop when all intact fibers are carrying loads that are below their failure thresholds. The number of fibers breaking between two successive load increments is called an avalanche size. To model a propagating interface, all fibers broken during the avalanche are then restored with zero initial load and a threshold value for failure drawn from the same distribution function as before. The load on the system is then increased, on all fibers equally, until the next breaking happens and an avalanche starts, and the dynamics continue. The timescale of avalanche is considered to be much smaller than the external loading rate, which enables us to consider a constant value for load during an ongoing avalanche.

The load redistribution process is considered to be distance dependent, i.e., if the i th fiber is broken, the fraction of the load received by the j th fiber is proportional to $\frac{1}{|i-j|^\gamma}$, where $\gamma = 0$ is the limit of equal load sharing (mean field) and $\gamma \rightarrow \infty$ is the local load-sharing limit. In practice, as noted elsewhere [39], $\gamma \approx 3$ is sufficient for the model to exhibit local load-sharing behavior.

We simulate for different values of γ and record the corresponding avalanches for the system size $L = 10\,000$ and measure the inequalities of such avalanches, as mentioned above.

2. Simulating qKPZ and qEW

In the Edward-Wilkinson equation and Kardar-Parisi-Zhang equation, we simulate the behavior of a one-dimensional interface model with quenched (q) noise. We use these two models to simulate the surface growth and evolution of a discrete interface represented by the height variable $h_i(t)$, and the growth rule for the discrete interface model is

$$h_i(t+1) = \begin{cases} h_i(t+1) & \text{if } G_i > 0 \\ h_i(t) & \text{otherwise,} \end{cases} \quad (15)$$

where

$$G_i = h_{i+1}(t) + h_{i-1}(t) - 2h_i(t) + \eta(i, h) + F \quad (16)$$

for EW, and

$$G_i = h_{i+1}(t) + h_{i-1}(t) - 2h_i(t) + \frac{1}{2} \left[\frac{h_{i+1}(t) - h_{i-1}(t)}{2} \right]^2 + \eta(i, h) + F \quad (17)$$

for KPZ, where $\eta(i, h)$ is the random δ correlated pinning force and F is the external driving force. Initially, the height profile of interface h_i is 0 and the periodic boundary conditions are used on the system size L . The height of the interface at each site h_i is updated using Eqs. (16) and (17) [46,47]. The pinning force η is randomly selected from a uniform distribution in the range $(-2, 2)$ in the case of the EW equation and $(-5, 5)$ in the case of the KPZ equation. Any change in that will be explicitly mentioned in the relevant places.

The simulation proceeds by applying the minimum external driving force on the interface, which is required to move the height of the interface. When the external driving force is smaller than the pinning force, the interface is pinned. When G_i is positive, the height of the interface h_i is moved by 1 and again new pinning forces, drawn from the same distribution, are assigned to the sites. This process continues until no more growth occurs or the local growth rate becomes zero. During this process, the external driving force has remained unchanged, and then it is increased again to restart the dynamics. The number of updated sites in between two stable states is the avalanche size S . When the external driving force is stronger than the critical value, the interface moves indefinitely, i.e., it is depinned.

IV. SIMULATION RESULTS

Here we explain the behavior of inequality indices g and k of the avalanche time series in the case of EW, KPZ, and fiber bundle interface model. The codes used for these simulations and the measurements of inequality indices are freely available in Ref. [48].

In Fig. 2(a), we have plotted the size distribution of avalanche size, denoted as $P(S)$ for the fiber bundle interface model prior to depinning. The size distributions are shown for various values of γ including 0, 0.5, 1, 1.5, 2, 2.5, 3, 3.5, 4, 4.5, and 5. Here, a low value of γ (< 2) signifies the mean-field interaction, while a high value of γ signifies the nearest-neighbor interaction. We observe a continuous variation in the exponent value of the size distribution δ ranging from 2.5 to 1.3 as γ varies from 0 to 5. In Fig. 2(b), we see that $\gamma = 2$ is the point beyond which the size distribution exponent δ is below 2. This is in line with earlier results in Ref. [39]. The end values of the indices, denoted by g_f and k_f , depend on the distribution of avalanche size exponent δ . When these avalanches are arranged in ascending order based on their sizes, the resulting curve will exhibit a divergence characterized by an exponent n , where $n = \frac{1}{\delta-1}$ for $n > 1$, and g_f and k_f will converge to 1 [35]. If the size distribution exponent δ remains below 2, then the divergence exponent will always be above 1.

Figure 3(a) shows the temporal evolution of g and k for various γ values, including 0, 1, 2, 3, 4, and 5, in the FBM. We observe that when γ is low (reflecting a mean-field regime), with a corresponding size distribution exponent δ of 2.5, g

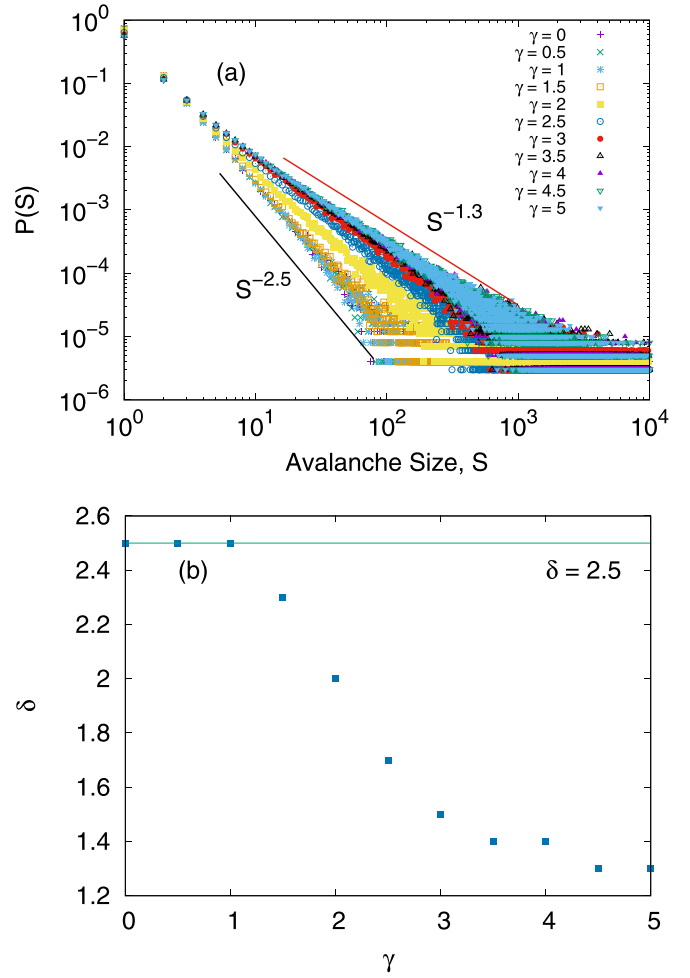


FIG. 2. (a) The avalanche size (prior to depinning) distribution $P(S)$ for the fiber bundle interface model is plotted for the different values of $\gamma = 0, 0.5, 1, 1.5, 2, 2.5, 3, 3.5, 4, 4.5$, and 5 for the system size $L = 10000$. (b) The variation of the size distribution exponent δ with γ . It can be seen that the avalanche size distribution exponent becomes steeper than 2 for $\gamma < 2$.

and k do not cross. This implies that in the mean-field limit, predicting depinning becomes challenging. However, when γ exceeds 2 (indicating the localized regime), the size distribution exponent δ (magnitude) decreases to 1.3, and the crossing of g and k is seen.

Now the problem for $\gamma < 2$ can also be solved if we simply take the time series of S^2 . Since its size distribution will be shallower, we will again see the crossing of g and k . In Figure 3(b), we square the avalanche size before computing the values of g and k . We observe that the crossing of g and k occurs consistently across all values of γ . We could have taken an even higher power of S (S^3, S^4 , etc.) to ensure the crossing of g and k . But the crossing would happen for an earlier value of σ , as the power is increased. So, the precision in the precursory signals would decay with the power used in the avalanche series.

As mentioned earlier, the expressions in Eqs. (12) and (14) assume monotonic variation of avalanche sizes with time (or load). But in individual samples of simulations, this does not hold. The approximation, therefore, can make a difference

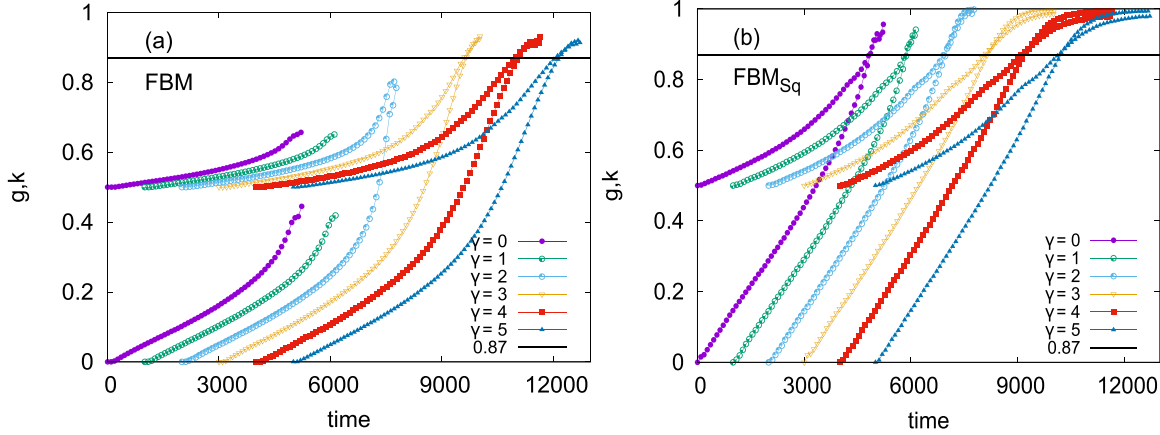


FIG. 3. The time variation of g and k is shown for the different values of $\gamma = 0, 1, 2, 3, 4,$ and 5 for the system size $L = 10000$ in the FBM interface. Here low γ corresponds to the mean-field limit and high γ corresponds to the localized load-sharing regime. (a) The crossing of g and k is seen when the γ value is high since the size distribution exponent value is lower there (see Fig. 2). (b) The crossing of g and k is always seen for all values of γ when we calculate g and k by taking the square of the avalanche sizes (i.e., S^2) because the size distribution of S^2 will have a smaller exponent value than that of S . However, for the γ values for which crossing was already happening for S , with S^2 the crossing happens slightly earlier. Note that for visual clarity, all curves, except $\gamma = 0$, are shifted in time.

between the actual crossing point of g and k and that estimated using the approximation. In order to see that such deviations do not critically affect the framework’s ability to produce precise precursory signals for different models, we extend this analysis to two additional models of depinning transition, namely, the EW and KPZ models. To begin our analysis, we first measure the size distribution exponents, denoted as δ , for these two models. The size distribution exponent is consistently 1.3 for EW and 1.4 for KPZ (see Fig. 4 inset). Then we calculate g and k using the time series data of avalanches, and in Fig. 4 we can see that the crossing of g and k occurs in both of these cases. This suggests that the crossing of g and k holds significant promise as an effective early indicator preceding the depinning transition in these two models as well.

To underline the fact that this crossing point of g and k happens at a point (say, σ^*) that is always before the critical point (say, σ_c), we calculate the probability distribution of the $Q(\frac{\sigma_c - \sigma^*}{\sigma_c})$ of the reduced variable $\frac{\sigma_c - \sigma^*}{\sigma_c}$ for all three models

(FBM, EW, KPZ) to check how far the crossing of g and k is happening from the depinning transition point (see Fig. 5). Here, σ_c represents the critical load at which depinning initiates and σ^* signifies the point at which g and k cross. Here in the fiber bundle interface model, we take the values of $\gamma = 4$ and 5 . In the EW model, we take two sets: in set 1, we choose a threshold distribution in the range $(-2, 2)$, while in set 2, we extend the range to $(-2.5, 2.5)$. In the KPZ model, for set 1, we consider the threshold distribution in the range $(-5, 5)$, and for set 2, we consider it to be $(-6, 6)$. In all the cases, we consistently observe that the crossing of g and k occurs at a distance of about 10% to 30% prior to the depinning transition point, underscoring its robustness as a predictive indicator. All the points of the expected g_{\min} and k_{\min} values are indicated in Fig. 1(b). It is also to be noted that in no case does the x -axis range go below zero, implying that in every single realization the crossing happened prior to the depinning, for all the models and pinning distributions considered here.

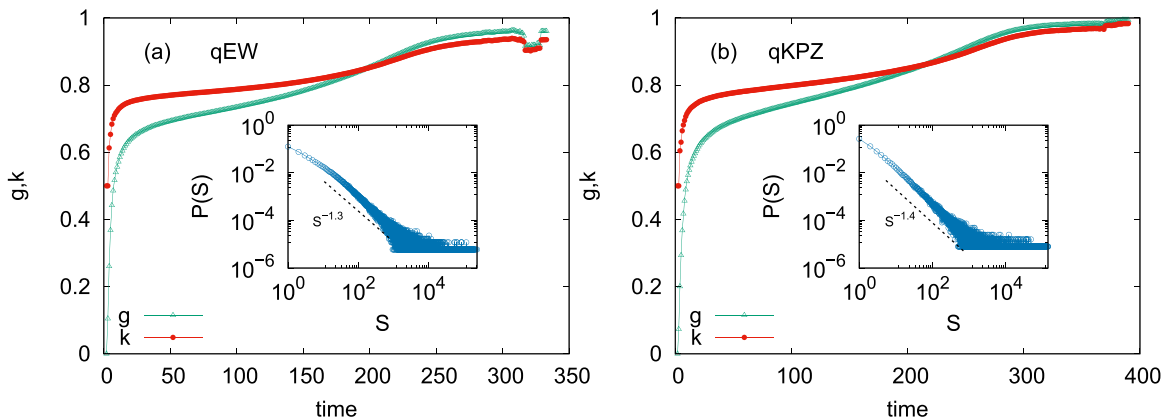


FIG. 4. The variation of g and k plotted with time for the two models, Edward-Wilkinson and Kardar-Parisi-Zhang, for the system size $L = 1000$. In the case of these two models, the crossing of g and k for different distributions of pinning forces (see text) is shown. Insets: The size distributions of the avalanches prior to depinning. The exponent values are always less than 2.

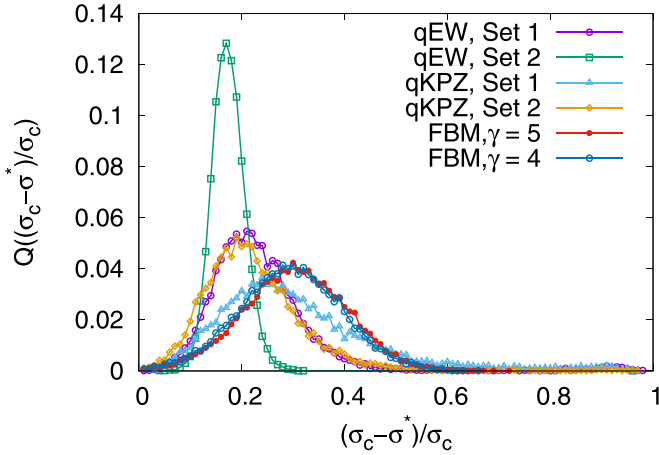


FIG. 5. The probability distributions of the $\frac{(\sigma_c - \sigma^*)}{\sigma_c}$ are shown for the three different models (quenched Edwards-Wilkinson model, quenched Kardar-Parisi-Zhang model, and fiber bundle interface model) for different threshold distributions. Here, σ_c is the critical load, i.e., the depinning point, and σ^* is the point where g and k cross. In the EW model, we consider two sets: in set 1, we take the threshold distribution to be uniform in the range $(-2, 2)$, and in set 2, we choose the threshold distribution to be uniform in the range $(-2.5, 2.5)$. In the KPZ model, in set 1, we take the threshold distribution to be uniform in the range $(-5, 5)$, and in set 2, we take the threshold distribution to be uniform in the range $(-6, 6)$. In the FBM, we take the two values of $\gamma = 4, 5$ and the threshold distribution to be uniform in $(0, 1)$. As can be seen, the distribution shows the peak in between 0.1 and 0.3, which means g and k cross near 10% to 30% away from the depinning transition point and therefore give a reliable indication of the imminent depinning transition. Here the averages are done over 10 000 ensembles.

V. DISCUSSION AND CONCLUSION

Forecasting the depinning transition point in interfaces driven through disordered media is an important problem. From catastrophic fracture propagation to magnetization switching, such questions are relevant to physicists and engineers alike. Generally, such cooperative intermittent dynamics leading to catastrophic changes have been subjected to investigations through various rule-based (see, e.g., [12–16,19,34]) and machine-learning (see, e.g., [17,18,20,29]) studies. In rule-based investigations, there are often strong sample-to-sample fluctuations, and in cases of machine-learning studies, there is a lack of a training set of experiments.

In this work, we study this question through the behavior of inequality indices traditionally used in social sciences. The Gini (g) and Kolkata (k) indices show remarkably stable characteristics prior to the depinning transition point, when measured using the unequal avalanches of the systems. Recall that the avalanches noted here are not in the stationary state, but in the nonstationary precritical state, where the average size of the avalanche grows with time (i.e., the applied load, assuming fixed loading rate). Given a power-law size distribution of the avalanches, it is possible to calculate the approximate expressions for the above two indices [see Eqs. (12) and (14)]. Then, when the time variation of the indices is looked at, they tend to cross each other at a point prior to the depinning threshold [see Fig. 1(a)]. Note that this

phenomenon is not just an average or most probable event, but something that happens on every single realization of all the models (fiber bundle, EW, and KPZ) studied here. Figure 5 indeed shows the distribution of the relative distance from the depinning point at which such crossing happened. It is consistently before the critical point in each case.

As the analytical estimates indicated, for steep enough size distributions (e.g., fiber bundle interface with $\gamma < 2$), such crossings do not happen. In that case, however, one can consider the square of the avalanche sizes, which will have a much shallower distribution and will therefore show a crossing in g and k . The functional form is hard to estimate since the second moment is not convergent in such cases for fiber bundles.

Finally, it is worth noting that the value at which the two indices cross is near universal (about 0.87) (see Fig. 3). This is seen from the analytical estimates and also from the numerical simulations of different models. Therefore, the signature of the precursor is not only widely applicable, but also near universal. Indeed, in other contexts, such near-universality was noted in simulations and data analysis, which are the results of the size distribution, as noted in Eqs. (12) and (14). In conclusion, we have outlined a framework for forecasting the imminent depinning transition in a wide variety of interfaces driven through disordered media, using social inequality indices. The indices, g and k , will cross each other at a time prior to the transition point. The analytical estimate and numerical simulations indicate that the precursory signals are near universal for all such depinning models and are obeyed in every realization of the simulations performed on Edwards-Wilkinson, Kardar-Parisi-Zhang, and fiber bundle interfaces. For a sufficiently global range of interactions, when g and k of the avalanches do not cross, if the indices are measured using the square of the avalanche sizes, then the crossing happens again. This indicates that for all realistic cases, by taking a sufficiently higher power of avalanche sizes, one can use the framework of precursory signals proposed here. An analysis using experimental data could be a fruitful future direction.

ACKNOWLEDGMENTS

The simulations were done using HPCC Surya in SRM University-AP. The authors are thankful to B. K. Chakrabarti for useful comments on the manuscript.

APPENDIX: INEQUALITY MEASURES FOR THE AVALANCHE TIME SERIES: GINI (G) AND KOLKATA (K) INDICES

In this Appendix, we explore the characteristics of the avalanche time series of the fiber bundle model (FBM), the quenched Edwards-Wilkinson (qEW) model, and the quenched Kardar-Parisi-Zhang (qKPZ) model. These time series exhibit a power-law distribution $P(S) \sim S^{-\delta}$, where the probability of large avalanches is few and small avalanches are more common. The exponent value δ remains consistent across various system sizes and threshold distributions, representing a universal property. However, the critical load required for the system depinning is not universal and strongly depends on the details of the system. Recently, it

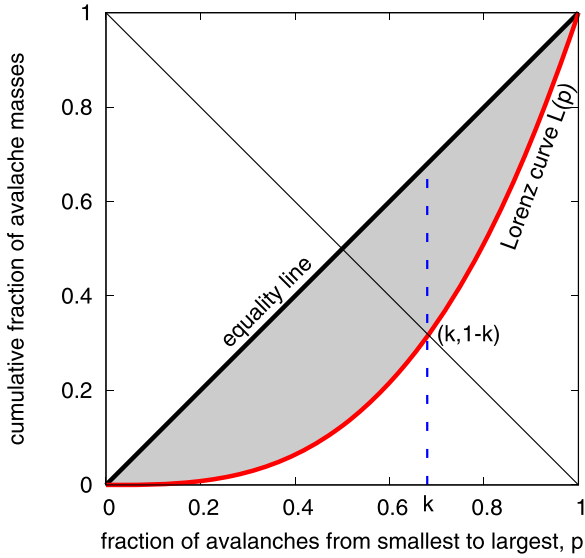


FIG. 6. A schematic diagram of the Lorenz function $\mathcal{L}(p)$, where $\mathcal{L}(p)$ denotes the cumulative fraction of the avalanche mass contained in the smallest p fraction of avalanches. If all avalanches were equal, this would be a diagonal straight line, called the equality line (indicated in the figure). The area between the equality line and the Lorenz curve (shaded area), therefore, is a measure of the inequality in the avalanche sizes. Two quantitative measures of such inequality are extracted from here: the ratio of the shaded area and that under the equality line (called the Gini index, g) and the crossing point of the opposite diagonal—from $(0,1)$ to $(1,0)$, shown in the dashed line, and the Lorenz curve, giving the Kolkata index k . The $1 - k$ fraction of the largest avalanches contains a k fraction of the cumulative avalanche mass.

has been shown [42] that some time-dependent inequality indices that tend to converge to seemingly universal values near the transition point can be derived from measuring the inequality among precritical avalanche sizes. Historically, some of those are over a century old, but used mainly in estimating economic inequality (e.g., Gini index [32]), and some of them have been recently introduced, such as the

Kolkata index [33]. Monitoring these quantities can serve as a valuable indicator to predict impending failure points.

In the following section of the Appendix, we provide a detailed explanation of how these parameters are defined from the avalanche time series.

The Lorenz function, Gini (g) and Kolkata (k) indices, and their approximate estimates

In the simulation of the FBM, EW, and KPZ interfaces, the time series of the avalanches can be arranged in the ascending order of their sizes. Then the Lorenz function $\mathcal{L}(p)$ gives the cumulative fraction of the avalanche mass (sum of all avalanche sizes) held by the p fraction of the smallest avalanches up to time t . It is important to note that if all avalanches were of equal size, then the Lorenz function would be a straight line starting from the origin and increasing linearly up to 1. This linear curve is known as the equality line (see Fig. 6). However, since the avalanches typically have varying sizes, the Lorenz function is nonlinear, staying below the equality line and monotonically increasing, with the constraints that $\mathcal{L}(p = 0) = 0$ and $\mathcal{L}(p = 1) = 1$. The area between the equality line and the Lorenz function shown as a shaded region in Fig. 6 serves as a measure of the inequality in avalanche sizes. The ratio of this area and that under the equality line ($1/2$ by construction) is called the Gini index g , which can be calculated by Eq. (12).

On the other hand, the ordinate value of the crossing point of the opposite diagonal [the straight line connecting points $(0,1)$ to $(1,0)$] provides the value of the Kolkata index k , which estimates the fraction $1 - k$ of the avalanches that collectively account for the fraction k of the total avalanche mass up to that time. The value of the k index is evaluated through Eq. (14).

As can be seen from Fig. 7, when the avalanches are kept in their order of occurrence and when they are arranged in the ascending order of their sizes, they do not vary too much. Particularly, the crossing points of g and k are similar. Therefore, the approximation made in the calculations [in writing Eq. (5)] when the avalanches are assumed to be in ascending order is good enough.

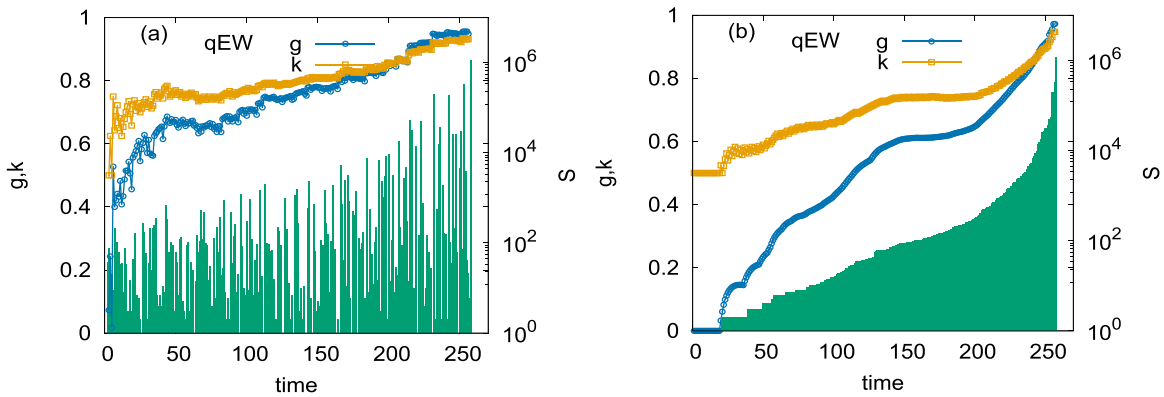


FIG. 7. (a) The time variation of the avalanche series (in logarithmic scale) along with g and k are plotted for the Edward-Wilkinson model (as a prototype). (b) The same avalanches along with g and k are shown when the avalanches are arranged in the ascending order of their sizes. Note that in the second case, the time is not the actual time order of the occurrences of the avalanches. The two figures show that as far as the crossing point values of g and k are concerned, it is a fair approximation to consider the size-ordered series for analytical estimates.

- [1] S. Zapperi, P. Cizeau, G. Durin, and H. E. Stanley, Dynamics of a ferromagnetic domain wall: Avalanches, depinning transition, and the Barkhausen effect, *Phys. Rev. B* **58**, 6353 (1998).
- [2] D. A. Huse and C. L. Henley, Pinning and roughening of domain walls in Ising systems due to random impurities, *Phys. Rev. Lett.* **54**, 2708 (1985).
- [3] M. Cieplak, M. O. Robbins, Dynamical transition in quasistatic fluid invasion in porous media, *Phys. Rev. Lett.* **60**, 2042 (1988).
- [4] M. A. Rubio, C. A. Edwards, A. Dougherty, and J. P. Gollub, Self-affine fractal interfaces from immiscible displacement in porous media, *Phys. Rev. Lett.* **63**, 1685 (1989).
- [5] A. I. Larkin and Yu. N. Ovchinnikov, Pinning in type II superconductors, *J. Low Temp. Phys.* **34**, 409 (1979).
- [6] D. S. Fisher, M. P. A. Fisher, and D. A. Huse, Thermal fluctuations, quenched disorder, phase transitions, and transport in type-II superconductors, *Phys. Rev. B* **43**, 130 (1991).
- [7] J. P. Bouchaud, E. Bouchaud, G. Lapasset, and J. Planès, Models of fractal cracks, *Phys. Rev. Lett.* **71**, 2240 (1993).
- [8] L. O. Eastgate, J. P. Sethna, M. Rauscher, T. Creteigny, C.-S. Chen, and C. R. Myers, Fracture in mode I using a conserved phase-field model, *Phys. Rev. E* **65**, 036117 (2002).
- [9] R. Toussaint and S. R. Pride, Interacting damage models mapped onto Ising and percolation models, *Phys. Rev. E* **71**, 046127 (2005).
- [10] A. L. Barabási and H. E. Stanley, *Fractal Concepts in Surface Growth*, (Cambridge University Press, Cambridge, 1995), p. 366.
- [11] S. Das, A. Zaig, H. Nhalil, L. Avraham, M. Schultz, and L. Klein, Switching of multi-state magnetic structures via domain wall propagation triggered by spin-orbit torques, *Sci. Rep.* **9**, 20368 (2019).
- [12] J. Koivisto, M. Ovaska, A. Miksic, L. Laurson and M. J. Alava, Predicting sample lifetimes in creep fracture of heterogeneous materials, *Phys. Rev. E* **94**, 023002 (2016).
- [13] L. Viitanen, M. Ovaska, S. K. Ram, M. J. Alava, and P. Karppinen, Predicting creep failure from cracks in a heterogeneous material using acoustic emission and speckle imaging, *Phys. Rev. Appl.* **11**, 024014 (2019).
- [14] S. Lennartz-Sassinek, I. G. Main, M. Zaiser and C. C. Graham, Acceleration and localization of subcritical crack growth in a natural composite material, *Phys. Rev. E* **90**, 052401 (2014).
- [15] A. Saichev and D. Sornette, Andrade, Omori, and time-to-failure laws from thermal noise in material rupture, *Phys. Rev. E* **71**, 016608 (2005).
- [16] F. Kun, I. Varga, S. Lennartz-Sassinek and I. G. Main, Approach to failure in porous granular materials under compression, *Phys. Rev. E* **88**, 062207 (2013).
- [17] E. D. Cubuk, S. S. Schoenholz, J. M. Rieser, B. D. Malone, J. Rottler, D. J. Durian, E. Kaxiras, and A. J. Liu, Identifying structural flow defects in disordered solids using machine-learning methods, *Phys. Rev. Lett.* **114**, 108001 (2015).
- [18] V. Bapst, T. Keck, A. Grabska-Barwińska, C. Donner, E. D. Cubuk, S. S. Schoenholz, A. Obika, A. W. R. Nelson, T. Back, D. Hassabis, and P. Kohli, Unveiling the predictive power of static structure in glassy systems, *Nat. Phys.* **16**, 448 (2020).
- [19] S. Papanikolaou, Microstructural inelastic fingerprints and data-rich predictions of plasticity and damage in solids, *Comput. Mech.* **66**, 141 (2020).
- [20] S. Biswas, D. F. Castellanos, and M. Zaiser, Prediction of creep failure time using machine learning, *Sci. Rep.* **10**, 16910 (2020).
- [21] D. Bonamy and E. Bouchaud, Failure of heterogeneous materials: A dynamic phase transition? *Phys. Rep.* **498**, 1 (2011).
- [22] S. Ben-Zeev, E. Aharonov, R. Toussaint, S. Parez, and L. Goren, Compaction front and pore fluid pressurization in horizontally shaken drained granular layers, *Phys. Rev. Fluids* **5**, 054301 (2020).
- [23] J. P. Sethna, K. A. Dahmen, and C. R. Myers, Crackling noise, *Nature (London)* **410**, 242 (2001).
- [24] S. Pradhan and B. K. Chakrabarti, Precursors of catastrophe in the Bak-Tang-Wiesenfeld, Manna, and random-fiber-bundle models of failure, *Phys. Rev. E* **65**, 016113 (2001).
- [25] G. Zöller, S. Hainzl, and J. Kurths, Observation of growing correlation length as an indicator for critical point behavior prior to large earthquakes, *J. Geophys. Res.* **106**, 2167 (2001).
- [26] M. Scheffer, S. Carpenter, T. Lenton, J. Bascompte, W. Brock, V. Dakos, J. van de Koppel, I. van de Leemput, S. Levin, E. van Nes, M. Pascual, and J. Vandermeer, Anticipating critical transitions, *Science* **338**, 344 (2012).
- [27] I. Morales, E. Landa, C. Angeles, J. Toledo, A. Rivera, J. Temis, and A. Frank, Behavior of early warnings near the critical temperature in the two-dimensional Ising model, *PLOS ONE* **10**, e0130751 (2015).
- [28] A. Noble, T. Rosenstock, P. Brown, J. Machta, and A. Hastings, Spatial patterns of tree yield explained by endogenous forces through a correspondence between the Ising model and ecology, *Proc. Natl. Acad. Sci. USA* **115**, 1825 (2018).
- [29] Diksha and S. Biswas, Prediction of imminent failure using supervised learning in a fiber bundle model, *Phys. Rev. E* **106**, 025003 (2022).
- [30] S. Banerjee, S. Biswas, B. K. Chakrabarti, S. K. Challagundla, A. Ghosh, S. R. Guntaka, H. Koganti, A. R. Kondapalli, R. Maiti, M. Mitra, and D. R. S. Ram, Evolutionary dynamics of social inequality and coincidence of Gini and Kolkata indices under unrestricted competition, *Intl. J. Mod. Phys. C* **34**, 2350048 (2023).
- [31] M. O. Lorenz, Methods of Measuring the Concentration of Wealth, *Publ. Am. Stat. Assoc.* **9**, 209 (1905).
- [32] C. Gini, Measurement of inequality of incomes, *Econ. J.* **31**, 124126 (1921).
- [33] A. Ghosh, N. Chattopadhyay, and B. K. Chakrabarti, Inequality in societies, academic institutions and science journals: Gini and k-indices, *Physica A* **410**, 30 (2014).
- [34] Diksha, S. Kundu, B. K. Chakrabarti, and S. Biswas, Inequality of avalanche sizes in models of fracture, *Phys. Rev. E* **108**, 024101 (2023).
- [35] S. Das and S. Biswas, Critical scaling through Gini index, *Phys. Rev. Lett.* **131**, 157101 (2023).
- [36] S. S. Manna, S. Biswas, and B. K. Chakrabarti, Near universal values of social inequality indices in self-organized critical models, *Physica A* **596**, 127121 (2022).
- [37] S. F. Edwards and D. R. Wilkinson, The Surface Statistics of a Granular Aggregate, *Proc. R. Soc. London A* **381**, 1780 (1982).
- [38] M. Kardar, G. Parisi, and Y. C. Zhang, Dynamic scaling of growing interfaces, *Phys. Rev. Lett.* **56**, 889 (1986).
- [39] S. Biswas and L. Goehring, Interface propagation in fiber bundles: Local, mean-field and intermediate

- range-dependent statistics, *New J. Phys.* **18**, 103048 (2016).
- [40] F. T. Pierce, 32-X.-Tensile tests for cotton yarns v.-“The weakest link” theorems on the strength of long and of composite specimens, *J. Textile Inst. Trans.* **17**, T355 (1926).
- [41] V. Pareto and A. N. Page, *Translation of “Manuale di Economia Politica” (Manual of Political Economy)* (A. M. Kelley, New York, 1971).
- [42] S. Biswas and B. K. Chakrabarti, Social inequality analysis of fiber bundle model statistics and prediction of materials failure, *Phys. Rev. E* **104**, 044308 (2021).
- [43] S. Biswas and L. Goehring, Load dependence of power outage statistics, *Europhys. Lett.* **126**, 44002 (2019).
- [44] T. S. Biró, A. Telcs, M. Józsa, and Z. Néda, Gintropic scaling of scientometric indexes, *Physica A* **618**, 128717 (2023).
- [45] A. Ghosh and B. K. Chakrabarti, Do successful researchers reach the self-organized critical point? *Physics* **6**, 46 (2013).
- [46] J. M. Kim and H. Choi, Depinning transition of the quenched Edwards-Wilkinson equation, *J. Korean Phys. Soc.* **48**, S241 (2006).
- [47] H. S. Song and J. M. Kim, A discrete model of the quenched Kardar-Parisi-Zhang equation, *J. Korean Phys. Soc.* **51**, 1630 (2007).
- [48] The codes used for simulating the interfaces are available at <https://github.com/soumya-84/Interface> and the codes used for measuring the inequality indices are available at https://github.com/soumya-84/FBM_RFM.